The Astrophysical Journal, 717:496–502, 2010 July 1 doi:10.1088/0004-637X/717/1/496
© 2010. The American Astronomical Society. All rights reserved. Printed in the U.S.A.

HIGH-TEMPERATURE PHOTOCHEMISTRY IN THE ATMOSPHERE OF HD 189733b

M. R. Line[1], M. C. Liang[2,3,4], and Y. L. Yung[1]
[1] Division of Geological and Planetary Sciences, California Institute of Technology, Pasadena, CA 91125, USA; mrl@gps.caltech.edu, yly@gps.caltech.edu
[2] Research Center for Environmental Changes, Academia Sinica, Taipei, Taiwan; mcl@rcec.sinica.edu.tw
[3] Graduate Institute of Astronomy, National Central University, Jhongli, Taiwan
[4] Institute of Astronomy and Astrophysics, Academia Sinica, Taipei, Taiwan
Received 2010 April 19; accepted 2010 May 12; published 2010 June 15

ABSTRACT

Recent infrared spectroscopy of hot exoplanets is beginning to reveal their atmospheric composition. Deep within the planetary atmosphere, the composition is controlled by thermochemical equilibrium. Photochemistry becomes important higher in the atmosphere, at levels above ∼1 bar. These two chemistries compete between ∼1 and 10 bars in hot-Jupiter-like atmospheres, depending on the strength of the eddy mixing and temperature. HD 189733b provides an excellent laboratory in which to study the consequences of chemistry of hot atmospheres. The recent spectra of HD 189733b contain signatures of CH_4, CO_2, CO, and H_2O. Here we identify the primary chemical pathways that govern the abundances of CH_4, CO_2, CO, and H_2O in the cases of thermochemical equilibrium chemistry, photochemistry, and their combination. Our results suggest that the disequilibrium mechanisms can significantly enhance the abundances of these species above their thermochemical equilibrium value, so some caution must be taken when assuming that an atmosphere is in strict thermochemical equilibrium.

Key words: atmospheric effects – methods: numerical – planetary systems – planets and satellites: atmospheres – stars: individual (HD 189733b) – radiative transfer

Online-only material: color figures

1. INTRODUCTION

Of the more than 400 exoplanets discovered thus far, dozens of them are transiting hot exoplanets, dubbed "hot Jupiters," from which we can obtain limited spectral information. A variety of chemical species have been detected in hot-Jupiter atmospheres. These include atomic species such as sodium (Na; Charbonneau et al. 2002), atomic hydrogen (Vidal-Madjar et al. 2003), atomic carbon and oxygen (Vidal-Madjar et al. 2004), and the molecular species: CO, CO_2, H_2O, and CH_4 (Tinetti et al. 2007; Swain et al. 2009a, 2009b). The detection of these species allows us to begin to explore the chemical pathways that control the observed abundances of these species. The species so far identified suggest that hydrocarbon chemistry via CH_4 photolysis as well as oxygen and water reactions is important.

The primary chemical pathways that determine chemical abundances in our own solar system are thermoequilibrium chemistry and photochemistry. Ion chemistry may also be important in these hot, highly irradiated atmospheres as it is important in the upper atmospheres of our own solar system planets (Kim & Fox 1994; Friedson et al. 2005; Vuitton et al. 2009). Current atmospheric modeling of hot-Jupiter atmospheres typically assume an atmospheric chemical composition consistent with thermochemical equilibrium (Burrows et al. 1997; Fortney et al. 2005, 2010; Sharp & Burrows 2007; Marley et al. 2007; Showman et al. 2009; Rogers et al. 2009; O'Donovan et al. 2010). Photochemical or other disequilibrium mechanisms, such as quenching, have not received the same attention (see, however, Liang et al. 2003, 2004; Cooper & Showman 2006; Zahnle et al. 2009a, 2009b). Thermoequilibrium chemistry occurs in high temperature and pressure regimes where chemical timescales are shorter than potential disequilibrium mechanisms, typically occurring deep within the planetary atmosphere (Yung & DeMore 1999, p. 135). Abundances are determined solely by the thermodynamic properties of compounds in the system via the minimization of the Gibbs free energy (Yung & DeMore 1999, pp. 56 and 135). Photochemistry is a disequilibrium process due to UV alteration by the host star. Photochemistry therefore should be important in hot-Jupiter atmospheres, given their proximity to their host stars (Liang et al. 2003).

Liang et al. (2003) were the first to explore the photochemistry that may occur on highly irradiated giant planets through modeling the sources of atomic hydrogen in HD 209458b. However, some of the rate coefficients used in that study are unsuitable for these high-temperature regimes, and several key reactions governing the production and loss of H_2O and CO_2 were not included. Additionally, better estimates of temperature and vertical transport profiles can be obtained from more sophisticated general circulation model (GCM) simulations.

Zahnle et al. (2009a, 2009b) explored products of sulfur photochemistry and how they may be responsible for the strong UV absorbers that cause thermal inversions as well as the formation of hydrocarbon soot. So far there have been no detections of sulfur species on these hot Jupiters.

The goal of this investigation is to understand the chemistry that produces the observed abundances of $\sim 10^{-5}$–10^{-3}, $\sim 10^{-6}$–10^{-3}, 10^{-5}–10^{-3}, and $\sim 10^{-6}$–10^{-7} for CO, CO_2, H_2O, and CH_4, respectively, as derived from the dayside emission spectrum of HD 189733b (Swain et al. 2009a; Madhusudhan & Seager 2009), by combining separate photochemical and thermochemical models and then comparing the results to simulations using photochemistry/thermochemistry alone. Furthermore, it has been recently suggested by Madhusudhan & Seager (2009) that there may be as much as 700 ppm of CO_2 present in the atmosphere of HD 189733b. The discrepancy between this value and the value from Swain et al. (2009a) is due to the assumed vertical distribution of CO_2 in the atmosphere (constant versus high concentration at one pressure level), which is not well constrained. This discrepancy suggests that there is much degeneracy in retrieving temperature and mixing ratio profiles, and that the exact values of the mixing ratios, or their vertical distributions, of the detected species are not well

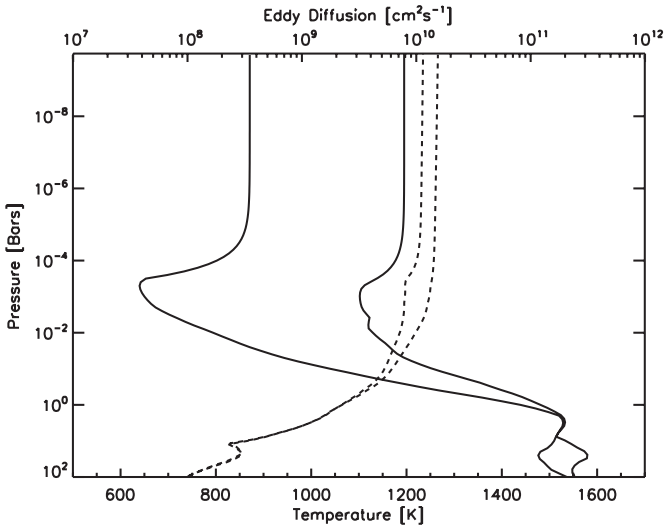

Figure 1. Temperature (solid) and eddy diffusion (dashed) profiles for the model atmosphere. The cooler temperature profile is taken from 30°N from the nightside of the model by Showman et al. (2009). The hotter temperature profile is taken from the dayside at the same latitude. The larger eddy diffusion is estimated as discussed in the text (the larger values are for the dayside). Eddy diffusion is read along the top axis; temperature is read along the bottom axis.

known. In this study, we identify the important mechanisms that govern the abundance of these detected species and their vertical distribution, using HD 189733b as an example.

2. MODELING

We use both a thermochemical model and a photochemical model to explain the observed abundances of CO, CO_2, H_2O, and CH_4 in the atmosphere of HD 189733b. The inclusion of sulfur or nitrogen species (e.g., see Zahnle et al. 2009a, 2009b) is beyond the scope of this paper and will be explored in later studies. Currently, we want to understand the effects that temperature and eddy mixing have on the photochemically derived mixing ratios. We adopt a hot profile representative of dayside temperatures and a cool profile representative of nightside temperatures for 30° N from Showman et al. (2009; Figure 1). We assume isothermal profiles above the upper boundary of the Showman et al. (2009) GCM for the sake of simplicity. These two profiles appear to have a thermal inversion near 1 mbar with a day–night contrast of ∼500 K. The use of two *T*–*P* profiles will illuminate the day/night contrast of the modeled species. Though HD 189733b is not expected to have an inversion, we still choose these *T*–*P* profiles because they span the range of hot-Jupiter temperature profiles in the literature (Fortney et al. 2006; Tinetti et al. 2007; Burrows et al. 2008), and the existence of an inversion does not affect the major chemical pathways.

In order to determine the thermoequilibrium abundances we use the chemical equilibrium with applications model developed by Gordon & McBride (1994). These abundances at the appropriate lower boundary (explained later) will be used for our lower mixing ratio boundary condition in the photochemical model. Thermochemical calculations require only pressure and temperature along with the relative molar mixing ratios of the atomic species involved in the compounds of interest, in this case C, O, and H (no N or S because they have not yet been detected). For the sake of simplicity, and in the absence of any other information, we assume solar abundance of these species ([C]/[H] $\sim 4.4 \times 10^{-4}$, [O]/[H] $\sim 7.4 \times 10^{-4}$, where [*i*] denotes the concentration of species *i* (Yung & DeMore 1999, p. 112). The thermochemical model computes the abundances of all possible compounds formed by those atomic species via a Gibbs free energy minimization routine (Gordon & McBride 1994). We compute the equilibrium abundances at each pressure–temperature level for our chosen temperature profiles. We would expect to see thermochemical equilibrium abundances in an atmosphere that does not undergo any dynamical or photochemical alterations, or where chemical timescales are much shorter than any disequilibrium timescales (Prinn & Barshay 1977; Smith 1998; Cooper & Showman 2006).

To compute the photochemical abundances of the species of interest, we use the Caltech/JPL-KINETICS one-dimensional photochemical model (Allen et al. 1981; Yung et al. 1984; Gladstone et al. 1996; Moses et al. 2005) for HD 189733b. HD 189733b is in a 2.2 day period orbiting at 0.03 AU around a K2V star. We use the UV stellar spectrum from HD 22049 which is also a K2V star (Segura et al. 2003). This K2V star has ∼2 orders of magnitude less flux below ∼3000 Å than the solar spectrum used in Zahnle et al. (2009a, 2009b), giving significantly different results. The model computes the abundances for 32 species involving H, C, and O in 258 reactions including 41 photolysis reactions and includes both molecular and eddy diffusion. The model uses the same hydrocarbon and oxygen chemistry as in Liang et al. (2003, 2004) but with high-temperature rate coefficients for the key reactions involved in the production and loss of H, CH_4, CO_2, CO, OH, and H_2O. The reaction rates given in the remainder of this paper are taken from Baulch et al. (1992) unless otherwise noted. We have also added two key reactions involved in the destruction of H_2O and CO_2. We have not, however, added a complete suite of reactions in order to achieve thermochemical equilibrium kinetically (e.g., Visscher et al. 2010). We do not expect this omission to invalidate our results, as we have included the key chemical pathways that govern the production and loss of the species of interest. The model atmosphere for the photochemical model uses the two temperature profiles described above. The lower boundary of the photochemical model is important in determining the mixing ratios throughout the atmosphere. We will estimate this lower boundary using quench level arguments rather than arbitrarily choosing some level. For more details on quench level estimation, we refer the reader to Prinn & Barshay (1977), Smith (1998), and Cooper & Showman (2006).

Eddy and molecular diffusion are key parameters determining the quench level and the distribution of the abundances in the atmosphere. Eddy diffusion is the primary vertical transport mechanism in our one-dimensional model. The strength of vertical mixing will determine where in the atmosphere the species become chemically quenched, and thus defines the lower boundary conditions for the photochemical model (Prinn & Barshay 1977; Smith 1998). Following Prinn & Barshay (1977), the transport timescale is given by

$$\tau_{\rm trans} \cong \frac{L^2}{K_z}, \quad (1)$$

where *L* is a vertical length scale typically chosen to be the scale height and K_z is the eddy diffusion coefficient. The chemical loss timescale of species *i* is given by

$$\tau_{{\rm chem},i} = \frac{[i]}{L_i}, \quad (2)$$

where $[i]$ is the concentration of species i and L_i is the loss rate of species i, typically determined by the bottleneck reaction. The quench level for species i is defined where $\tau_{\rm trans} = \tau_{{\rm chem},i}$. For levels where $\tau_{\rm trans} < \tau_{{\rm chem},i}$ the mixing ratio of species i is fixed at the quench level value. For levels below the quench level, the compounds reach thermochemical equilibrium.

In order to determine the quench level in the atmosphere of HD 189733b, we must first estimate the strength of eddy mixing and the timescale for the conversion of CO to CH_4 (Prinn & Barshay 1977; Griffith & Yelle 1999). The eddy diffusion profile adopted in this model is derived from a globally root-mean-squared (rms) averaged vertical wind profile from a GCM (A. Showman 2010, private communication) and is estimated by

$$K_z \sim wL, \tag{3}$$

where w is the rms average of the vertical wind velocity. Smith (1998) suggests that the appropriate length scale is some fraction of the scale height. Here we assume that it is the scale height, thus giving us an upper limit on eddy diffusion. The GCM-derived rms-averaged vertical winds range from 0 (at ~200 bars) to 7 m s^{-1} (~0.8 mbar). The vertical wind is assumed to be constant above this height. Combining this with a typical scale height of ~200 km gives an eddy diffusion of $\sim 10^{10}$ cm^2 s^{-1} (Figure 1). Typical transport timescales from Equation (1) are on the order of $\sim 10^5$ s.

The rate-limiting step in the conversion of CO to CH_4, and thus the reaction determining the chemical lifetime of CO, is

$$\mathrm{H + H_2CO + M \rightarrow CH_3O + M} \tag{4}$$

(Yung et al. 1988; Griffith & Yelle 1999; Cooper & Showman 2006). The rate coefficient in reaction (4) has not been measured in the lab, but its high-pressure (~1 bar) reverse reaction rate has been measured to be

$$k_r = 1.4 \times 10^{-6} T^{-1.2} e^{-7800/T} \ \mathrm{cm^6\ s^{-1}}, \tag{5}$$

where T is the temperature at which the reaction takes place (Page et al. 1989). If we assume the high-pressure limit, which is reasonable for where quenching is expected to occur, Equation (4) k_f can be estimated via

$$\frac{k_f}{k_r} = K_{\rm eq} = e^{(G_f - G_r)/RT}, \tag{6}$$

where $K_{\rm eq}$ is the equilibrium constant for the net thermochemical reaction (Yung et al. 1988)

$$\mathrm{H + H_2CO \leftrightarrow CH_3O}, \tag{7}$$

where G_f and G_r are the Gibbs free energies of the reaction, given respectively by $H[\mathrm{H}] + H[\mathrm{H_2CO}] - T(S[\mathrm{H}] + S[\mathrm{H_2CO}])$ and $H[\mathrm{CH_3O}] - TS[\mathrm{CH_3O}]$, with $H[\mathrm{X}]$ being the enthalpy of formation of species X, and $S[\mathrm{X}]$ being the entropy of species X. The enthalpies and entropies of the given species are taken to be at 1000 K and can be found at http://www.grc.nasa.gov/WWW/CEAWeb/ceaThermoBuild.htm. With the relevant thermochemical data and Equations (5) and (6), we can estimate the forward reaction rate of reaction (4) to be

$$k_f = 3.07 \times 10^{-12} T^{-1.2} e^{3927/T}. \tag{8}$$

The CO chemical lifetime can then be determined using

$$\tau_{\rm chem} \sim \frac{[\mathrm{CO}]}{k_f [\mathrm{H}][\mathrm{H_2CO}]}, \tag{9}$$

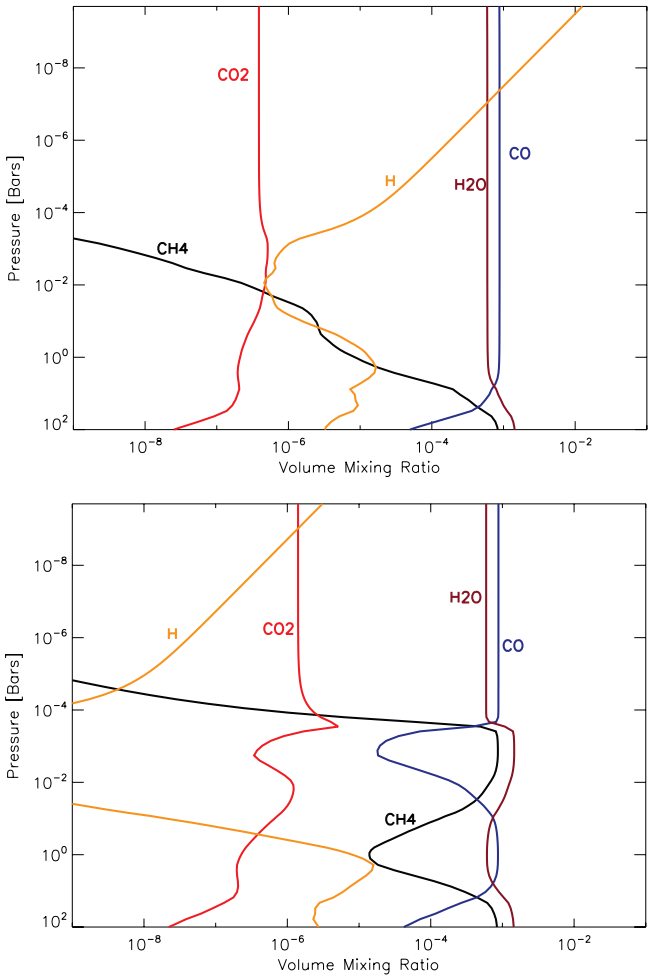

Figure 2. Thermochemical equilibrium mixing ratios derived from the temperature profiles in Figure 1. Top: mixing ratios derived for the dayside (hotter) profile. Bottom: mixing ratios derived for the (nightside) cooler profile.

(A color version of this figure is available in the online journal.)

where the concentrations of CO, H, and H_2CO are determined via the thermochemical model. Upon equating Equation (9) with Equation (1) using the dayside temperature profile we determine the quench level, and thus the lower boundary, to be ~3 bars (~1530 K) which is similar to the results of Cooper & Showman (2006) for HD 209458b. This pressure level is much higher than that of Jupiter (~100 bars; Prinn & Barshay 1977) and is similar to that of brown dwarfs (~6 bars; Griffith & Yelle 1999). Choosing a length scale less than the scale height as suggested by Smith (1998) can move the quench level to a higher pressure. This is because the chemical timescale in Equation (9) increases with increasing altitude and lower temperature. Using a length scale of $0.1H$ instead of H moves the quench level to ~8 bars, at where there is very little change in the thermochemical mixing ratios from ~3 bars (Figure 2). Additionally, there is no significant difference in quench level between the nightside and dayside because the two T–P profiles converge near the quench level.

We assume a zero concentration gradient at the lower boundary in order to allow photochemical products to sink down into the deeper atmosphere except for the observed species of CO, H_2O, CH_4, and CO_2. For these species we fix the mixing ratios to be the thermochemically derived values at the ~3 bar quench level: 8.41×10^{-4}, 6.36×10^{-4}, 4.09×10^{-5}, and

1.96×10^{-7}, respectively, for the dayside and 8.39×10^{-4}, 6.38×10^{-4}, 4.25×10^{-5}, and 1.98×10^{-7}, respectively, for the nightside. We assume a zero flux boundary condition for the top of the atmosphere, i.e., little or no atmospheric escape, though this assumption may not be entirely true for atomic hydrogen (Vidal-Madjar et al. 2003). This assumption has a negligible effect on the results.

3. RESULTS

3.1. Thermochemical Results

The thermochemically derived mixing ratios (relative to H_2) are shown in Figure 2. Again, these are the expected mixing ratios if there were no dynamical or photochemical process occurring in the atmosphere, which we know not to be true. If we focus first on the dayside profiles, we can see that CO is the dominant carbon bearing species and remains relatively constant with altitude as do H_2O and CO_2. We also note that CH_4 falls off rapidly with increasing altitude (decreasing pressure). We can understand this result by noting that CO, CH_4, and H_2 abundances are related through the net thermochemical reactions

$$CH_4 + H_2O \leftrightarrow CO + 3H_2 \quad (10)$$

$$CO + H_2O \leftrightarrow CO_2 + H_2. \quad (11)$$

Then by Le Chatelier's principle, as the total partial pressure of the atmosphere decreases, the system will want to resist that decrease in order to maintain equilibrium by producing more molecules (smaller molecules), which in this case results in the production of CO and H_2. Upon comparing the dayside profiles to the cooler nightside profile, we note that CH_4 becomes more abundant. CH_4 is more energetically favorable at lower temperatures and is much more sensitive to the effects of temperature than CO and CO_2. We also note that atomic hydrogen is more abundant at warmer temperatures than at cooler temperatures due to the entropy term in the Gibbs free energy. From a thermochemical perspective, we can expect $\sim$10 mbar mixing ratios of the observable species, CO, H_2O, CH_4, and CO_2, to range from (2–9) $\times 10^{-4}$, (6–13) $\times 10^{-4}$, (2.6–6758) $\times 10^{-7}$, and (4.7–16) $\times 10^{-7}$, respectively, due to the day/night contrast. For comparison, the measured values from Swain et al. (2009a) and Madhusudhan & Seager (2009) for CO, H_2O, CH_4, and CO_2 are, respectively, $\sim 10^{-4}$–10^{-2}, 10^{-5}–10^{-3}, $\sim 10^{-7}$, and 10^{-6}–10^{-3}.

3.2. Photochemical Results

We run four cases of our photochemical model (Figure 3) in order to compare the effects of temperature and photolysis versus no photolysis on the mixing ratios (relative to H_2) for H, CO, H_2O, CO_2, and CH_4. In the following subsections, we will discuss the important reactions governing the production and loss of each of the relevant species.

3.2.1. H_2O, OH, and H

The primary reactions that govern the production and loss of H_2O are

R71: $H_2O + h\nu \rightarrow H + OH \quad J_{71} = 2.587 \times 10^{-8}\ s^{-1}$ (1 mbar)

R137: $OH + H_2 \rightarrow H_2O + H \quad k_{137} = 1.70 \times 10^{-16}\, T^{1.6}\, e^{-1660/T}\ cm^3\ s^{-1}$

R254: $H + H_2O \rightarrow OH + H_2 \quad k_{254} = 7.50 \times 10^{-16}\, T^{1.6}\, e^{-9718/T}\ cm^3\ s^{-1}$.

R137 and R254 are fast enough to readily recycle each other so that the abundance of H_2O remains relatively constant with altitude at a quench level value of $\sim 6.36 \times 10^{-4}$ below the homopause at $\sim$10 nbar. The photolysis of H_2O does not significantly affect its abundance in the observable atmosphere as can be seen in Figure 3 because the loss timescale of H_2O when struck by photolysis is everywhere longer than the transport timescale, thus allowing recently photolyzed parcels to be readily replenished by upwelling. The photolysis of H_2O, however, does produce the important OH and H radicals that drive the remainder of the chemistry (Figure 4), with the net result being the conversion of H_2 to 2H.

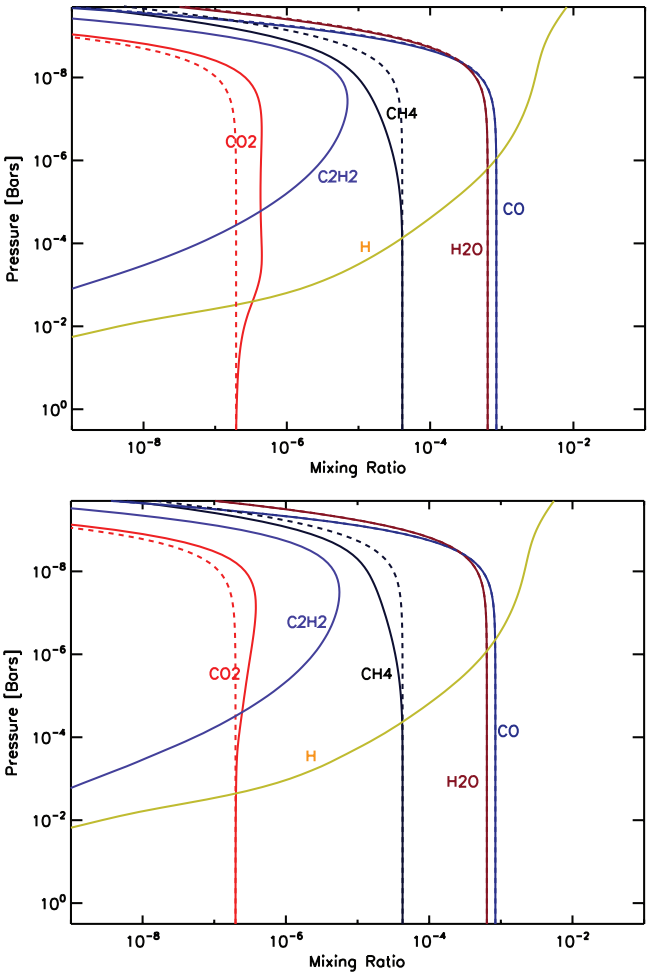

Figure 3. Photochemical mixing ratios (solid) compared to the case with no photochemistry and only quenching (dashed) for the day (top) and night (bottom) temperature profiles. The dashed curves on the bottom plot are representative of what may be seen on the night side of the planet. Note that there is virtually no H or C_2H_2 for the cases in which photochemistry is turned off (e.g., the dashed curves for these species are not in the plot range).

(A color version of this figure is available in the online journal.)

H_2O photodissociates into OH and H at wavelengths lower than 2398 Å. For HD 189733b, below this wavelength there are $\sim 2 \times 10^{15}$ photons $cm^{-2}\ s^{-1}$ available for H_2O photolysis. For comparison, the UV flux below this wavelength at Jupiter is $\sim 7 \times 10^{12}$ photons $cm^{-2}\ s^{-1}$ and for HD 209458b, $\sim 10^{17}$ photons $cm^{-2}\ s^{-1}$. OH and H increase with increasing altitude due to the availability of more UV photons. The production of H at high altitudes via H_2O photolysis may be the driver of hydrodynamic escape on hot Jupiters (Liang et al. 2003).

In short, the abundance of H_2O is primarily set by the thermochemical equilibrium value at the lower boundary condition,

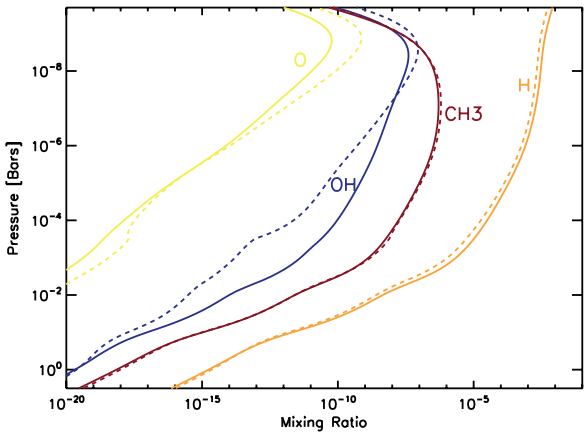

Figure 4. Important radical species involved in pathways governing the abundances of CH_4, H_2O, CO, and CO_2. Solid is for the dayside temperature profile, dashed is for the nightside temperature profile. The abundances of radicals increase with decreasing pressure due to the availability of dissociating photons higher in the atmosphere.

(A color version of this figure is available in the online journal.)

taken here to be the quench level, and rapidly decreases with altitude above the homopause. If the quench level changes, the observable value of H_2O will change but not significantly, as can be seen in Figure 2. The derived value here is slightly higher than the Swain et al. (2009a) dayside emission observations of (0.1–1) $\times 10^{-4}$ but is more consistent with the value obtained by the Tinetti et al. (2007) terminator observations of $\sim 5 \times 10^{-4}$. The day to night contrast is nearly unnoticeable in Figure 3.

3.2.2. CO & CO_2

Thermochemically, CO is the dominant carbon reservoir in hot atmospheres above ~10 bars (Figure 2). The abundance of CO is set by the quench level thermochemical equilibrium abundance of 8.4×10^{-4}. The abundance of CO_2 is determined via the interconversion of oxygen from the large reservoirs of CO and H_2O into CO_2 via the OH radical. Deeper down in the atmosphere, say, below the quench level, or in the presence of weak vertical transport (low eddy diffusion), oxygen is moved into CO_2 via the following reactions:

R137: $\mathrm{OH + H_2 \rightarrow H_2O + H}$ $k_{137} = 1.70 \times 10^{-16}\, T^{1.6}\, e^{-1660/T}$ cm^3 s^{-1}

R152: $\mathrm{OH + CO \rightarrow CO_2 + H}$ $k_{152} = 1.05 \times 10^{-17}\, T^{1.5}\, e^{250/T}$ cm^3 s^{-1}

R254: $\mathrm{H + H_2O \rightarrow OH + H_2}$ $k_{254} = 7.50 \times 10^{-16}\, T^{1.6}\, e^{-9718/T}$ cm^3 s^{-1}

R255: $\mathrm{H + CO_2 \rightarrow OH + CO}$ $k_{255} = 2.51 \times 10^{-10}\, e^{-13350/T}$ cm^3 s^{-1}.

R152 is the reaction that gives the oxygen from H_2O and CO to CO_2. There is no net production or loss of species from these reactions, meaning they will assume thermochemical equilibrium. Assuming steady state, these four reactions can be combined to give the kinetically achieved thermochemical mixing ratio of CO_2 in terms of the rate constants (k) and mixing ratios (f) of the large reservoirs of CO and H_2O:

$$f_{CO_2} \sim \frac{k_{152}k_{254}}{k_{137}k_{255}} f_{H_2O} f_{CO} = 1.85 \times 10^{-7} T^{1.5} e^{5542/T} f_{H_2O} f_{CO}. \quad (12)$$

This relation would determine the mixing ratio of CO_2 in the absence of any disequilibrium mechanisms such as photochemistry or quenching. Using the thermochemical mixing ratios of H_2O ($\sim 6 \times 10^{-4}$) and CO ($\sim 9 \times 10^{-4}$) and evaluating the rate constants at the daytime temperature ($T \sim 1200$ K) we obtain a CO_2 mixing ratio of $\sim 4 \times 10^{-7}$, which is consistent with Figure 2.

In the photochemical limit (in the absence of eddy mixing), the photolysis reactions, R71 and R75, become more important and effectively replace R254 and R255, so the important chain of reactions becomes

R137: $\mathrm{OH + H_2 \rightarrow H_2O + H}$ $k_{137} = 1.70 \times 10^{-16}\, T^{1.6}\, e^{-1660/T}$ cm^3 s^{-1}

R152: $\mathrm{OH + CO \rightarrow CO_2 + H}$ $k_{152} = 1.05 \times 10^{-17}\, T^{1.5} e^{250/T}$ cm^3 s^{-1}

R71: $\mathrm{H_2O} + h\nu \rightarrow \mathrm{H + OH}$ $J_{71} = 2.587 \times 10^{-8}$ s^{-1} (1 mbar)

R75/76: $\mathrm{CO_2} + h\nu \rightarrow \mathrm{CO + O}$ $J_{75/76} = 4.4 \times 10^{-10}$ s^{-1} (1 mbar)

Net: $\mathrm{OH + H_2 \rightarrow 3H + O}$.

Combining these reactions allows us to estimate the photochemical mixing ratio of CO_2 with

$$f_{CO_2} \sim \frac{k_{152}J_{71}}{k_{137}J_{75+76}} f_{H_2O} f_{CO} = 0.062 T^{-0.1} e^{1910/T} \frac{J_{71}}{J_{75+76}} f_{H_2O} f_{CO}, \quad (13)$$

where J is the photolysis rate of the indicated photolysis reaction. As an extreme case, we assume that the top of atmosphere photolysis rate of H_2O is $\sim 10^{-5}$ s^{-1}, the photolysis rate of CO_2 is $\sim 5 \times 10^{-8}$ s^{-1}, and the dayside temperature is ~1200 K, giving an upper limit of ~few $\times 10^{-5}$ for f_{CO_2}. Equation (13) suggests that the abundance of CO_2 is photochemically enhanced rather than reduced. The abundance of CO_2 in the presence of only quenching (no photochemistry) will remain fairly constant below the homopause at ~1 nbar (Figure 3). This is due to the lack of excess OH produced in R71 used to drive R152 to produce CO_2. Again, for comparison, the observed mixing ratio of CO_2 from Swain et al. (2009a) and Madhusudhan & Seager (2009) range from $\sim 10^{-6}$ to 10^{-3}.

3.2.3. CH_4 and Heavier Hydrocarbons

The primary fate of CH_4 in the upper atmosphere is reaction with H to produce CH_3, which immediately reacts with H_2 to restore CH_4,

R28: $\mathrm{CH_4 + H \rightarrow CH_3 + H_2}$ $k_{28} = 2.20 \times 10^{-20}\, T^3\, e^{-4041/T}$ cm^3 s^{-1}

R53: $\mathrm{CH_3 + H_2 \rightarrow CH_4 + H_2}$ $k_{53} = 1.14 \times 10^{-20}\, T^{2.7}\, e^{-4739/T}$ cm^3 s^{-1}.

The result is a closed loop. However, the above recycling is not perfect, and the following sequence of reactions occur in the upper atmosphere:

R28: $2 \times [\mathrm{CH_4 + H \rightarrow CH_3 + H_2}]$ $k_{28} = 2.20 \times 10^{-20}\, T^3\, e^{-4041/T}$ cm^3 s^{-1}

R4: $2 \times [\mathrm{CH_3} + h\nu \rightarrow \mathrm{CH_2 + H}]$ $J_{28} = 1.95 \times 10^{-3}$ s^{-1} (1 mbar)

R48: $\mathrm{CH_2 + CH_2 \rightarrow C_2H_2 + 2H}$ $k_{48} = 1.80 \times 10^{-10} \times e^{-400/T}$ cm^3 s^{-1} (Bauerle et al. 1995)

Net: $\mathrm{2CH_4 \rightarrow C_2H_2 + 2H_2 + 2H}$.

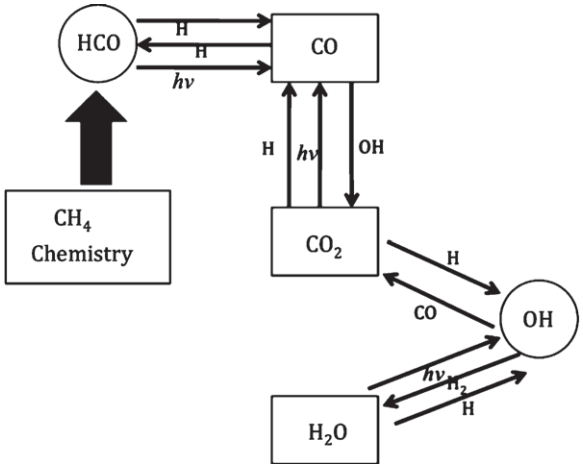

Figure 5. Photochemical web illustrating the important chemical pathways that govern the production and loss of the observable species. The boxes represent the observed species and the circles represent species yet to be observed but are key in the production and loss of the observed constituents.

The net result is the production of C_2H_2 in the upper atmosphere at the ~1 ppm level. No other C_2 hydrocarbons are produced in significant quantities. The primary fate of C_2H_2 from the upper atmosphere is downward transport, followed by hydrogenation back to CH_4. The abundance of CH_4 is $\sim 4 \times 10^{-5}$, which is several orders of magnitudes larger than the $\sim 10^{-7}$ detected by Swain et al. (2009a) and used by Liang et al. (2003), but is more consistent with the terminator observations of CH_4 giving mixing ratios of up to 5×10^{-5} (Swain et al. 2008). The abundance of CH_4 produced via quenching is also many orders of magnitude larger than the expected thermochemical equilibrium values (see Figures 2 and 3) with very little thermochemically derived CH_4 ($<10^{-9}$) present above 0.1 mbar.

4. DISCUSSION

We have analyzed the important disequilibrium mechanisms, photochemistry, and simple dynamical quenching that govern the vertical distribution of the observed species in hot-Jupiter atmospheres. The important chemical pathways that govern the abundances of the observable species are illustrated in Figure 5. With the exception of methane, our derived abundances are consistent with the observations of Swain et al. (2009a). We obtained a value of $\sim 4 \times 10^{-5}$, while the observations suggest two orders of magnitude less (Swain et al. 2009a). The observed value of $\sim 10^{-7}$ corresponds to the thermochemical equilibrium value at ~10 mbar. This would mean that the quench level would have to be at this pressure, suggesting an eddy diffusion on the order of $\sim 10^3$ cm^2 s^{-1} from Equations (9) and (1). Alternatively, it may be possible that the observations are probing above the homopause where the mixing ratio can be substantially less than $\sim 10^{-5}$ (Figure 3). Our value of methane is also several orders of magnitude larger than reported by Liang et al. (2003) for HD 209458b. This is because the temperature at the lower boundary used by Liang et al. (2003) for HD 209458b is ~700 K hotter than our lower boundary temperature of ~1530 K and methane is less stable at higher temperatures. The vertical profile for CH_4 derived here falls off much slower than that in Zahnle et al. (2009a). This is because the K2V UV flux used in this investigation is ~2 orders of magnitude less than the solar UV flux used in Zahnle et al. (2009a). The more UV photons available, as there would be around a solar type G star, the greater the destruction of CH_4, and hence the greater the production of C_2H_2.

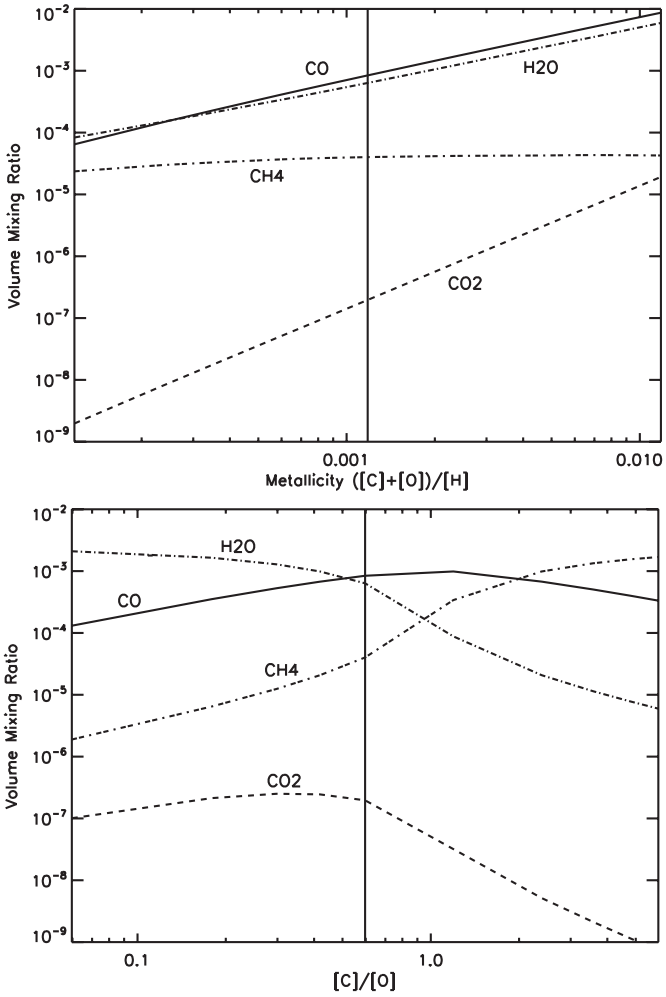

Figure 6. Effects of changing metallicity (top) and C/O ratio (bottom) on the 3 bar quench level mixing ratios for CO, H_2O, CO_2, and CH_4. The vertical lines in each plot represent the solar values.

The metallicity of these hot Jupiters is not well constrained. Swain et al. (2009a) suggest that the metallicity for HD 189733b may be subsolar and that the [C]/[O] ratio is between 0.5 and 1. We assumed solar metallicity, but we can explore what might happen if this is not the case. Changes in metallicity will affect the thermochemical equilibrium abundances. This will in turn change the lower boundary mixing ratios. We varied the metallicity (taken here to be ([C]+[O])/[H]) from one-tenth solar up to ten times solar to see what effect it would have on our lower boundary mixing ratios (Figure 6). The thermochemical mixing ratios of CO, H_2O, and CO_2 vary by several orders of magnitude over the range of metallicities, where as CH_4 changes very little. This orders of magnitude change at the lower boundary due to metallicity will affect our photochemical results by the same amount. With 10 times the solar metallicity we could expect mixing ratios of CO and H_2O to be as high as ~0.1 and CO_2 as high as 10^{-5}. CO_2 is more readily affected by metallicity than the other species because it has two oxygens as opposed to CO's one oxygen (Lodders & Fegley 2002; Zahnle et al. 2009a). Even higher metallicities will produce more extreme abundances of CO, CO_2, and H_2O.

The [C]/[O] ratio also affects the thermochemical abundances. Here, we vary the [C]/[O] ratio from 0.1 to 10 times

the solar ratio of ∼0.6 while keeping the overall metallicity ([C]+[O])/[H]) constant at the solar value (Figure 6). The mixing ratio of CO does not vary significantly, but can get as high as $\sim 10^{-3}$ given a slightly supersolar [C]/[O] ratio. CO_2 rapidly decreases for ratios above solar and can get as low as 0.1 ppb for 10 times the solar ratio. As the [C]/[O] ratio increases past 1, H_2O and CH_4 swap roles in taking up H and can change as much as 3 orders of magnitude.

There appears to be minor compositional variability between the nightside and dayside. Comparing the solid curves in the top panel of Figure 3 to the dashed curves in the bottom panel of Figure 3 gives some sense of the magnitude of the day–night variability. There are no dissociating photons on the nightside, so the quench level mixing and atmospheric circulation determine the abundance throughout the rest of the atmosphere below the homopause. There is a less than 1% maximum variability in CO and H_2O, a factor of ∼3 more CH_4 on the nightside over the dayside, and up to a factor of 2 more CO_2 on the dayside. CO_2 and CH_4 concentrations experience more variability because they are most affected by photochemical reactions that only occur on the dayside (CH_4 gets destroyed due to R141 and photolysis, CO_2 is enhanced via Equation (13)). C_2H_2 would exhibit much variability since it is produced strictly from photochemistry. We could expect to see up to 1 ppm on the dayside of these hot planets with very minute amounts on the nightside where it would be readily thermochemically recycled back to methane. Terminator observations should fall somewhere between the dayside and nightside values.

5. CONCLUSIONS

We have shown that both photochemistry and vertical quenching can significantly alter the abundances of CO_2, CH_4, and C_2H_2 in hot-Jupiter atmospheres. Vertical quenching determines the lower boundary values and thus the mixing ratios of CO and H_2O, which are not significantly affected photochemically. CO_2 can be photochemically produced above its quench level value by the reaction described in Equation (13), and CH_4 can be readily photochemically destroyed. However, as a whole, the vertical quenching primarily dictates the abundances of these species in the observable portion of the atmosphere. These ideas can be extended to other hot-Jupiter atmospheres, though we used HD 189733b as our test case. One can see from Equation (13) that the fate of CO_2 is determined by the temperature of the atmosphere and the ratio of the H_2O photolysis rate to the CO_2 photolysis rate, which all depend on the stellar type and the distance. Knowledge of these terms will allow us to predict the abundance of CO_2 in any hot-Jupiter atmosphere. Though we have not included sulfur and nitrogen species in this study as in Zahnle et al. (2009a, 2009b) we have still shown that simple C, O, and H chemistry and their interplay with vertical quenching are consistent with the detected abundances of CO, CH_4, CO_2, and H_2O. Finally, the vertical distribution of species derived from thermochemical equilibrium can deviate substantially from those derived via quenching, photochemistry, and diffusion, and the simple assumption of thermochemical equilibrium may not be valid in the observable regions of these atmospheres.

We especially thank Adam Showman for providing us his GCM outputs for temperature and vertical winds, both of which form the basis of our model atmosphere, making it possible for us to determine the eddy diffusion coefficient. We also thank Run-Li Shia, Giovanna Tinetti, Xi Zhang, Konstantin Batygin, Mimi Gerstell, Chris Parkinson, Vijay Natraj, Kuai Le, Mark Swain, Julie Moses, Wes Traub, Pin Chen, Gautam Vasisht, Nicholas Heavens, Heather Knutson, Sara Seager, the anonymous referee, and the Yuk Yung group for very useful discussions and for reading the manuscript. M.R.L. was supported by the JPL Graduate Fellowship (JPLGF). M.C.L. was supported in part by NSC grant 98-2111-M-001-014-MY3 to Academia Sinica. Y.L.Y. was supported by NASA grant NX09AB72G to the California Institute of Technology.

REFERENCES

Allen, M., Yung, Y. L., & Waters, J. W. 1981, J. Geophys. Res., 86, 3617
Bauerle, S., Klatt, M., & Wagner, H. Gg. 1995, Ber. Bunsenges. Phys. Chem., 99, 870
Baulch, D. L., et al. 1992, J. Phys. Chem. Ref. Data, 21, 411
Burrows, A., Budaj, J., & Hubeny, I. 2008, ApJ, 678, 1436
Burrows, A., et al. 1997, ApJ, 491, 856
Charbonneau, D., Brown, T. M., Noyes, R. W., & Gilliland, R. L. 2002, ApJ, 568, 377
Cooper, C. S., & Showman, A. P. 2006, ApJ, 649, 1048
Fortney, J. J., Marley, M. S., Lodders, K., Saumon, D., & Freedman, R. 2005, ApJ, 627, 69
Fortney, J. J., Saumon, D., Marley, M. S., Lodders, K., & Freedman, R. S. 2006, ApJ, 642, 495
Fortney, J. J., Shabram, M., Showman, A. P., Lian, Y., Freedman, R. S., Marley, M. S., & Lewis, N. K. 2010, ApJ, 709, 1396
Friedson, A. J., Wilson, E. H., & Moses, J. I. 2005, BAAS, 37, 683
Gladstone, G. R., Allen, M., & Yung, Y. L. 1996, Icarus, 119, 1
Gordon, S., & McBride, B. J. 1994, Computer Program for Calculation of Complex Chemical Equilibrium Compositions and Applications (NASA Reference Publication 1311; Cleveland, OH: NASA), http://www.grc.nasa.gov/WWW/CEAWeb/
Griffith, C. A., & Yelle, R. V. 1999, ApJ, 519, L85
Kim, Y. H., & Fox, J. L. 1994, Icarus, 112, 310
Liang, M. C., Parkinson, C. D., Lee, A. Y.-T., Yung, Y. L., & Seager, S. 2003, ApJ, 596, L247
Liang, M. C., Seager, S., Parkinson, C. D., Lee, A. Y.-T., & Yung, Y. L. 2004, ApJ, 605, L61
Lodders, K., & Fegley, B. 2002, Icarus, 155, 393
Madhusudhan, N., & Seager, S. 2009, ApJ, 707, 24
Marley, M. S., Fortney, J. J., Hubickyj, O., Bodenheimer, P., & Lissauer, J. J. 2007, ApJ, 655, 541
Moses, J. I., Fouchet, T., Bézard, B., Gladstone, G. R., Lellouch, E., & Feuchtgruber, H. 2005, J. Geophys. Res., 110, 8001
O'Donovan, F. T., Charbonneau, D., Harrington, J., Madhusudhan, N., Seager, S., Deming, D., & Knutson, H. A. 2010, ApJ, 710, 1551
Page, M., Lin, M. C., He, Y., & Choudhur, T. K. 1989, J. Phys. Chem., 93, 4404
Prinn, R. G., & Barshay, S. S. 1977, Science, 198, 1031
Rogers, J. C., Apai, D., López-Morales, M., Sing, D. K., & Burrows, A. 2009, ApJ, 707, 1707
Segura, A., Krelove, K., Kasting, J. F., Sommerlatt, D., Meadows, V., Crisp, D., Cohen, M., & Mlawer, E. 2003, Astrobiology, 3, 689
Sharp, C. M., & Burrows, A. 2007, ApJS, 168, 140
Showman, A. P., Fortney, J. J., Lian, Y., Marley, M. S., Freedman, R. S., Knutson, H. A., & Charbonneau, D. 2009, ApJ, 699, 564
Smith, M. D. 1998, Icarus, 132, 176
Swain, M. R., Vasisht, G. V., & Tinetti, G. 2008, Nature, 452, L329
Swain, M. R., Vasisht, G., Tinetti, G., Bouwman, J., Chen, P., Yung, Y., Deming, D., & Deroo, P. 2009a, ApJ, 690, L114
Swain, M. R., et al. 2009b, ApJ, 704, 1616
Tinetti, G., et al. 2007, Nature, 448, 169
Vidal-Madjar, A., Lecavelier des Etangs, A., Désert, J.-M., Ballester, G. E., Ferlet, R., Hébrard, G., & Mayor, M. 2003, Nature, 422, 143
Vidal-Madjar, A., et al. 2004, ApJ, 604, L69
Visscher, C., Moses, J. I., & Saslow, S. A. 2010, arXiv:1003.6077
Vuitton, V., Lavvas, P., Yelle, R. V., Galand, M., Wellbrock, A., Lewis, G. R., Coates, A. J., & Wahlund, J.-E. 2009, Planet. Space Sci., 57, 1558
Yung, Y. L., Allen, M., & Pinto, J. P. 1984, ApJS, 55, 465
Yung, Y. L., & DeMore, W. B. 1999, Photochemistry of Planetary Atmospheres (Oxford: Oxford Univ. Press)
Yung, Y. L., Drew, W. A., Pinto, J. P., & Friedl, R. R. 1988, Icarus, 73, 516
Zahnle, K., Marley, M. S., & Fortney, J. J. 2009a, arXiv:0911.0728
Zahnle, K., Marley, M. S., Freedman, R. S., Lodders, K., & Fortney, J. J. 2009b, ApJ, 701, L20